

Superconductor-insulator-ferromagnet-superconductor Josephson junction: From the dirty to the clean limit

N. G. Pugach,^{1,*} M. Yu. Kupriyanov,² E. Goldobin,³ R. Kleiner,³ and D. Koelle³

¹*Faculty of Physics, M.V. Lomonosov Moscow State University, 119992 Leninskie Gory, Moscow, Russia*

²*Skobeltsyn Nuclear Physics Institute, M.V. Lomonosov Moscow State University, 119992 Leninskie Gory, Moscow, Russia*

³*Physikalisches Institut–Experimentalphysik II and Center for Collective Quantum Phenomena, Universität Tübingen, Auf der Morgenstelle 14, D-72076 Tübingen, Germany*

(Dated: February 12, 2018)

The proximity effect and the Josephson current in a superconductor-insulator-ferromagnet-superconductor (SIFS) junction are investigated within the framework of the quasiclassical Eilenberger equations. This investigation allows us to compare the dirty and the clean limits, to investigate an arbitrary impurity scattering, and to determine the applicability limits of the Usadel equations for such structures. The role of different types of the FS interface is analyzed. It is shown that the decay length ξ_1 and the spatial oscillation period $2\pi\xi_2$ of the Eilenberger function may exhibit a nonmonotonic dependence on the properties of the ferromagnetic layer such as exchange field or electron mean free path. The results of our calculations are applied to the interpretation of experimentally observed dependencies of the critical current density on the ferromagnet thickness in Josephson junctions containing a Ni layer with an arbitrary scattering.

PACS numbers: 74.45.+c, 74.50.+r, 74.78.Fk

I. INTRODUCTION

Superconductor-ferromagnet-superconductor (SFS) Josephson junctions are a subject of intensive theoretical and experimental studies^{1–3}. In particular, the question of the applicability range of predictions from dirty and clean limit theories and the treatment of the crossover between these two limits has been recognized as an important problem for the theoretical description of SFS structures^{4,5}.

For the majority of experimental realizations of SFS structures^{6–15} the exchange energy H of the ferromagnetic materials is rather large^{10,14}. As a consequence, the characteristic magnetic length $\xi_H = \hbar v_f / 2H \lesssim \ell_f$, where ℓ_f is the electron mean free path and v_f is the Fermi velocity in the F layer^{6–15}. Under this condition the numerous theoretical predictions^{1–3} based on the Usadel equations¹⁶ have a rather restricted range of validity; i.e. a more general approach based on the Eilenberger equations¹⁷ has to be developed.

A simple expression for the critical current density J_C , which is valid in the clean limit, was derived in Ref. 18. Still the analysis of the Eilenberger equations for more general cases, remained a difficult problem. A significant progress along this direction has been achieved a decade ago⁴, where the solution of the Eilenberger equations for arbitrary scattering has been expressed in an integral form⁴. It was supposed⁴ that the SF interface transparency D is small enough, providing the opportunity to use the linearized equations. Thus, a general expression for the Josephson junction supercurrent has been derived and used for numerical evaluations. The integral representation of the solution of the Eilenberger equations also permits to reproduce analytical expressions for J_C obtained earlier within both clean and dirty limits^{6,18,19}. Recently, the same results have been achieved using the

Ricatti parametrization of the one-dimensional Eilenberger equations⁵. However, the obtained expressions⁴ are so complicated that they are difficult to analyze and use in practice. Although the use of a one-dimensional equation⁵ significantly simplifies the problem, it contains a non-controllable assumption about the insignificance of the angular distribution of the Eilenberger function.

Despite of this progress, it is still not clear within which range of parameters and with what accuracy it is possible to use simple expressions for the clean¹⁸ and dirty¹⁹ limits. The question about the influence of transport properties of SF interfaces is also still open. Since the answer to these questions is rather important for experimentalists, we formulate here a problem for a particular case of superconductor-insulator-ferromagnet-superconductor (SIFS) junctions. In comparison with SFS, in SIFS structures superconductivity is induced in the F layer only from one S electrode. This essentially simplifies the analysis compared to that for SFS junctions.

On the one hand, SIFS junctions are interesting by themselves as potential elements for superconducting logic circuits^{20–22} because it is possible to vary their critical current density in the π state within a rather wide range, still keeping a high $J_C R_N$ product^{12,23}, where R_N is the junction normal resistance per square. Furthermore, in comparison with SFS junctions, SIFS junctions have very small damping which decreases exponentially at $T \rightarrow 0$. This makes them useful for superconducting circuits where low damping is required. On the other hand, an SIFS junction represents a convenient model system for a comparative study of 0- π transitions for an arbitrary ratio of characteristic lengths in the F layer: the F-layer thickness d_f , the mean free path ℓ_f , the characteristic magnetic length ξ_H , and the nonmagnetic coherence length $\xi_0 = \hbar v_f / 2\pi k_B T$, where T is the temperature.

To calculate J_C of an SIFS junction, it is sufficient to study the proximity effect in the FS bilayer and to calculate the magnitude of the Eilenberger functions at the IF interface. For simplicity we will restrict ourselves to the study of the situation when the anomalous Green's function induced in the F layer is small enough, permitting us to use the linearized Eilenberger equation for the description of the superconducting properties induced in the ferromagnet. Such an approximation is valid if the FS interface has a small transparency or if T is close to the critical temperature T_c of the S electrodes.

This article is organized as follows. In sec. II we describe our model based on the linearized Eilenberger equation supplemented with Zaitsev boundary conditions²⁴ for an SIFS junction. Different types of FS boundaries are analyzed. Section III presents dependencies of anomalous Green's functions and the critical current density on the F-layer parameters. The comparison with experimental results is presented in Section IV. Section V concludes this work. The calculation details can be found in the Appendix.

II. MODEL

A. Proximity effect in the FS electrode

To analyze the proximity effect in an FS bilayer for arbitrary values of the electron mean free paths ℓ_s and ℓ_f in the S and F layer, respectively, it is convenient to introduce the following functions

$$\Phi_+ = \frac{1}{2} [f(x, \theta_s, \omega) + f^+(x, \theta_s, \omega)], \quad (1)$$

$$\Phi_- = \frac{1}{2} [f(x, \theta_s, \omega) - f^+(x, \theta_s, \omega)], \quad (2)$$

where $f(x, \theta_s, \omega)$ and $f^+(x, \theta_s, \omega)$ are the quasiclassical Eilenberger functions¹⁷. Then we rewrite the Eilenberger equations for the S layer, located at $0 \leq x \leq \infty$, in the form:

$$\frac{k_s^2}{\ell_s^2 \mu_s^2} \frac{\partial^2}{\partial x^2} \Phi_+ - \Phi_+ = -\frac{2\Delta\tau_s + \langle \Phi_+ \rangle}{2|\omega|\tau_s + 1}, \quad (3)$$

where

$$\langle \Phi_+ \rangle = \int_0^1 \Phi_+ d\mu, \quad (4)$$

$$\Phi_- = -\frac{\ell_s \text{sign}(\omega)}{k_s} \mu_s \frac{\partial}{\partial x} \Phi_+. \quad (5)$$

The insulating layer of negligible thickness is located at $x = -d_f$. In the F layer (located at $-d_f \leq x \leq 0$) the equations have the form

$$\frac{k_f^2}{\ell_f^2 \mu_f^2} \frac{\partial^2}{\partial x^2} \Phi_+ - \Phi_+ = -\frac{\langle \Phi_+ \rangle}{k_f}, \quad (6)$$

$$\Phi_- = -\frac{\ell_f \text{sign}(\omega)}{k_f} \mu_f \frac{\partial}{\partial x} \Phi_+. \quad (7)$$

Here $\omega = \pi T(2n + 1)$ are Matsubara frequencies, $\theta_{s,f}$ are the angles between the FS interface normal and the direction of Fermi velocities $v_{s,f}$ in the S and F layers, respectively, $\mu_{f,s} = \cos \theta_{f,s}$, Δ is the superconducting order parameter, which is assumed to be zero in the ferromagnet, $\tau_{s,f} = \ell_{s,f}/v_{s,f}$ are electron scattering times, and corresponding wave vectors $k_s = 2|\omega|\tau_s + 1$, $k_f = 2[|\omega| + iH \text{sign}(\omega)]\tau_f + 1 = 2|\omega|\ell_f/v_f + i2H\ell_f/v_f \text{sign}(\omega) + 1 = 1 + \ell_f/\xi_\omega + i \text{sign}(\omega)\ell_f/\xi_H$, $\xi_\omega = v_f/2|\omega|$. We use the units where $\hbar = 1$ and $k_B = 1$. Here we also take into account that the normal Eilenberger function in the ferromagnet $g \approx \text{sign}(\omega)$. We also neglect multiple reflections from the FS and the IF interfaces, which is reasonable if $d_f \geq \ell_f$, i.e. the ballistic regime is not considered. The fully ballistic case with a double barrier SIFS junction was examined in Ref. [25].

Equations (3)–(7) must be supplemented by the boundary conditions. At $x \rightarrow \infty$ the function Φ_+ should approach its bulk value

$$\Phi_+(\theta_s, \omega) = \frac{\Delta_0}{\sqrt{\Delta_0^2 + \omega^2}}, \quad (8)$$

where Δ_0 is the magnitude of superconductor order parameter far from the SF interface. At $x = -d_f$ the boundary condition

$$\frac{d}{dx} \Phi_+(-d_f, \theta_f, \omega) = 0 \quad (9)$$

guarantees the absence of a current across the insulating layer.

The boundary conditions at the FS interface strongly depend on its transport properties. Below we will assume for the FS interface transparency $D(\mu_f) \ll 1$. Then to the first approximation we may neglect the suppression of superconductivity in the S electrode and rewrite the Zaitsev boundary conditions²⁴ in the form

$$\frac{\ell_f}{k_f} \mu_f \frac{\partial}{\partial x} \Phi_+ = D(\mu_f) \frac{\Delta_0}{\sqrt{\Delta_0^2 + \omega^2}}. \quad (10)$$

From the structure of Eilenberger equations (3)–(7) and the boundary conditions (8)–(10) it follows that

$$\Phi_+(\theta_s, \omega) = \Phi_+(\theta_s, -\omega), \quad (11a)$$

$$\Phi_+(\theta_f, \omega) = \Phi_+^*(\theta_f, -\omega), \quad (11b)$$

$$\Phi_-(\theta_s, \omega) = -\Phi_-(\theta_s, -\omega), \quad (12a)$$

$$\Phi_-(\theta_f, \omega) = -\Phi_-(\theta_f, -\omega). \quad (12b)$$

These symmetry relations permit us to consider the solution of the boundary problem formulated above only for $\omega > 0$.

B. Solution of the Eilenberger equations in the F layer.

It is convenient to look for a solution of Eilenberger equations in the F layer (7) in the form

$$\Phi_+ = \sum_{m=-\infty}^{\infty} Q_m \cos\left(\frac{\pi m(x+d_f)}{d_f}\right) + B \cosh\left(\frac{x+d_f}{\ell_f |\mu_f|} k_f\right), \quad (13)$$

which automatically satisfies the boundary condition (9). The relation between the coefficients Q_m , and B can be

found by substitution of the ansatz (13) into the Eilenberger equation (6). Multiplying the obtained equations by $\cos[\pi k(x+d_f)/d_f]$, and integrating them over x , one can easily find the relation between the coefficients Q_m , and B , see the Appendix. $B = B(\mu_f)$ can be found from the boundary condition (10). Thus we arrive to the following expression for the Eilenberger function in the ferromagnet

$$\Phi_+ = \frac{\Delta_0}{\sqrt{\Delta_0^2 + \omega^2}} \left[\sum_{m=-\infty}^{\infty} \frac{\langle D(\mu) \frac{\mu}{q} \frac{(-1)^m}{M(\mu)} \rangle_{\mu}}{M(\mu_f) [k_f - \langle \frac{1}{M} \rangle]} \cos\left(\frac{\pi m(x+d_f)}{d_f}\right) + \frac{D(\mu_f)}{\sinh\left(\frac{q}{\mu_f}\right)} \cosh\left(\frac{x+d_f}{d_f \mu_f} q\right) \right], \quad (14)$$

where

$$q = \frac{d_f k_f}{\ell_f} = d_f \left(\frac{1}{\ell_f} + \frac{1}{\xi_{\omega}} + i \frac{1}{\xi_H} \right).$$

Then the Eilenberger function averaged over the angle θ_f has the form

$$\langle \Phi_+ \rangle = \frac{\Delta_0}{\sqrt{\Delta_0^2 + \omega^2}} \sum_{m=-\infty}^{\infty} \frac{\langle D(\mu) \frac{\mu}{q} \frac{(-1)^m}{M(\mu)} \rangle_{\mu}}{\left[k_f - \frac{q}{\pi m} \arctan\left(\frac{\pi m}{q}\right) \right]} \cos\left(\frac{\pi m(x+d_f)}{d_f}\right), \quad (15)$$

There are several interface models with a different $D(\mu_f)$ dependence.

First, the FS interface may be represented by a thick diffusive barrier. Then the incident electron scatters in any arbitrary direction with equal probability, independent on the incident angle, i.e.,

$$D(\mu_f) = D_1. \quad (16)$$

The second model considers an FS interface with a potential barrier, which appears due to different Fermi velocities in the S and F layer. The transmission coefficient in this case has the form

$$D(\mu_f) = \frac{4v_s \mu_s v_f \mu_f}{(v_s \mu_s + v_f \mu_f)^2} \approx \frac{4v_f}{v_s} \mu_f = D_2 \mu_f, \quad \text{if } v_s \gg v_f. \quad (17)$$

It is necessary to note, that the incidence angle and the reflection angle are related by the expression

$$v_s \sin \theta_s = v_f \sin \theta_f. \quad (18)$$

Therefore, only the electrons which are at almost normal incidence to the interface ($\mu_s \approx 1$) may penetrate through the barrier. This model seems to be mostly reasonable for description of recent experiments²⁶ with Nb electrodes ($v_s \sim 5 \dots 6 \cdot 10^7$ cm/s) and 3d ferromagnets or its Cu alloys²⁷ (for Ni $v_f \approx 2.8 \cdot 10^7$ cm/s).

Third, one can model the FS interface as a high and narrow (δ -function like) potential barrier between two metals with close Fermi-velocities. In this case

$$D(\mu_f) = \frac{4v_s \mu_s v_f \mu_f}{(v_s \mu_s + v_f \mu_f + W)^2} \approx \frac{4v_s v_f}{W^2} \mu_f^2 = D_3 \mu_f^2, \quad \text{if } v_s \approx v_f, \quad (19)$$

where W is the strength of δ -function like barrier.

For the above mentioned three models of the FS interface we have three possible expressions for Φ_+ with different average values $\langle \Phi_+ \rangle$, see (A7)-(A9) for details.

First, for $D(\mu_f) = D_1$

$$\Phi_+ = \frac{\Delta_0 D_1}{\sqrt{\Delta_0^2 + \omega^2}} \left[\sum_{m=-\infty}^{\infty} \frac{\frac{q}{2\pi^2 m^2} (-1)^m \ln \left[\frac{\pi^2 m^2}{q^2} + 1 \right] \cos \left(\frac{\pi m(x+d_f)}{d_f} \right)}{\left(m^2 \frac{\pi^2 \mu_f^2}{q^2} + 1 \right) \left[k_f - \frac{q}{\pi m} \arctan \left(\frac{\pi m}{q} \right) \right]} + \frac{\cosh \left(q \frac{x+d_f}{d_f \mu_f} \right)}{\sinh \left(\frac{q}{\mu_f} \right)} \right]. \quad (20)$$

Second, for $D(\mu_f) = \mu_f D_2$

$$\Phi_+ = \frac{\Delta_0 D_2}{\sqrt{\Delta_0^2 + \omega^2}} \left[\sum_{m=-\infty}^{\infty} \frac{\frac{q}{\pi^2 m^2} (-1)^m \left(1 - \frac{q}{\pi m} \arctan \frac{\pi m}{q} \right) \cos \left(\frac{\pi m(x+d_f)}{d_f} \right)}{\left(m^2 \frac{\pi^2 \mu_f^2}{q^2} + 1 \right) \left[k_f - \frac{q}{\pi m} \arctan \left(\frac{\pi m}{q} \right) \right]} + \frac{\mu_f \cosh \left(q \frac{x+d_f}{d_f \mu_f} \right)}{\sinh \left(\frac{q}{\mu_f} \right)} \right]. \quad (21)$$

Third, for $D(\mu_f) = \mu_f^2 D_3$

$$\Phi_+ = \frac{\Delta_0 D_3}{\sqrt{\Delta_0^2 + \omega^2}} \left[\sum_{m=-\infty}^{\infty} \frac{\frac{q}{2\pi^2 m^2} (-1)^m \left(1 - \frac{q^2}{\pi^2 m^2} \ln \left(\frac{\pi^2 m^2}{q^2} + 1 \right) \right) \cos \left(\frac{\pi m(x+d_f)}{d_f} \right)}{\left(m^2 \frac{\pi^2 \mu_f^2}{q^2} + 1 \right) \left[k_f - \frac{q}{\pi m} \arctan \left(\frac{\pi m}{q} \right) \right]} + \frac{\mu_f^2 \cosh \left(q \frac{x+d_f}{d_f \mu_f} \right)}{\sinh \left(\frac{q}{\mu_f} \right)} \right]. \quad (22)$$

These are the solutions of the linearized Eilenberger equation in the ferromagnet. The corresponding expressions for $\langle \Phi_+ \rangle$ are given by Eqs. (A11)-(A13) in the Appendix.

Let us consider how these expressions reproduce the limiting cases of strong and weak scattering, for which the solutions are well-known^{1,2}.

C. Dirty limit

If the electron mean free path is the smallest characteristic length i.e. $\ell_f \ll \xi_H, \xi_0, d_f$, the frequent nonmagnetic scattering permits averaging over the trajectories¹⁶. Then it is possible to write a closed system of equations for averaged functions. The linearization of the Usadel equations is allowed at the same conditions as for the Eilenberger equation.

The linearized Usadel equation in the ferromagnet has the form

$$\xi_f^2 \frac{\partial^2}{\partial x^2} \langle \Phi_+ \rangle + \frac{(\omega + iH)}{\pi T_c} \langle \Phi_+ \rangle = 0 \quad (23)$$

where $\xi_f^2 = D_f/2\pi T_c$, and $D_f = \ell_f v_f/3$ is the diffusion coefficient. The solution of Eq. (23) may be written as

$$\langle \Phi_+ \rangle = A \cosh \left(\frac{x - d_f}{\xi_f} \sqrt{\frac{\omega + iH}{\pi T_c}} \right) \quad (24)$$

The boundary condition at $x = 0$ reads²⁸

$$\gamma_B \xi_f \frac{\partial}{\partial x} \langle \Phi_+ \rangle = \frac{\Delta_0}{\sqrt{\Delta_0^2 + \omega^2}}. \quad (25)$$

Substituting the expression (24) into the Usadel equation (23) one can find the coefficient

$$A = \frac{\Delta_0}{\gamma_B \sqrt{\Delta_0^2 + \omega^2}} \frac{1}{\sqrt{\frac{\omega + iH}{\pi T_c}}} \frac{1}{\sinh \left(\frac{d_f}{\xi_f} \sqrt{\frac{\omega + iH}{\pi T_c}} \right)}. \quad (26)$$

Let us consider the previously obtained averaged Eilenberger function (15). For small ℓ_f the parameter q is large and

$$\begin{aligned} 1 + \ell_f/\xi_\omega + i\ell_f/\xi_H - \frac{q}{\pi m} \arctan \left(\frac{\pi m}{q} \right) &\approx \\ &\approx \frac{1}{3q^2} \left[\pi^2 m^2 + \frac{d_f^2}{\xi_f^2} \frac{(\omega + iH)}{\pi T_c} \right] \end{aligned}$$

It is seen that the sums in (14) and (15) converge at $\pi^2 m^2 \approx 2(\omega + iH) d_f^2/d_f$. At these values of m

$$\pi^2 m^2 \frac{\mu_f^2}{q^2} \approx \frac{2(\omega + iH)}{d_f} d_f^2 \frac{\mu_f^2}{d_f^2} \ell_f^2 \approx \frac{6(\omega + iH)}{v_f} \mu_f^2 \ell_f \ll 1$$

and

$$\Phi_+ \approx \frac{\Delta_0}{\sqrt{\Delta_0^2 + \omega^2}} \left[\sqrt{\frac{\pi T_c}{\omega + iH}} \frac{\cosh \left(\sqrt{\frac{\pi T_c}{\omega + iH}} \frac{x+d_f}{\xi_f} \right)}{\gamma_B \sinh \left(\sqrt{\frac{\pi T_c}{\omega + iH}} \frac{d_f}{\xi_f} \right)} + \frac{D(\mu_f)}{\sinh \left(\frac{q}{\mu_f} \right)} \cosh \left(q \frac{x+d_f}{d_f \mu_f} \right) \right], \quad (27)$$

where the suppression parameter γ_B describes the electron transmission through the FS interface, see expres-

sions (A14)–(A16). After averaging over θ_f the expression (27) coincides with (24) with A given by (26). It turns out that in the dirty limit the first term of the expression (14) for the Eilenberger function plays the main role, as the second term reduces due to the spatial averaging (15), and the Eilenberger function $\Phi_+ = \langle \Phi_+ \rangle$.

D. Clean limit

For a larger electron mean free path ℓ_f the sum in (A4) converges at

$$\pi^2 m^2 \frac{\mu_f^2}{q^2} \approx 1, \quad \frac{\pi m}{q} \approx \frac{1}{\mu_f}.$$

In the limit $\xi_H \ll \xi_\omega$ we have

$$k_f - \frac{q}{\pi m} \arctan\left(\frac{\pi m}{q}\right) \approx \ell_f/\xi_\omega + i\ell_f/\xi_H$$

and

$$\begin{aligned} \Phi_+ = \frac{\Delta_0}{\sqrt{\Delta_0^2 + \omega^2}} & \left\{ \left(\frac{\ell_f}{\xi_\omega} + \frac{i\ell_f}{\xi_H} \right)^{-1} \left\langle \frac{\mu D(\mu)}{\mu_f^2 - \mu^2} \left[\frac{\mu_f \cosh\left(\frac{qm(x+d_f)}{\mu_f d_f}\right)}{\sinh\frac{q}{\mu_f}} - \frac{\mu \cosh\left(\frac{qm(x+d_f)}{\mu d_f}\right)}{\sinh\frac{q}{\mu}} \right] \right\rangle_\mu \right. \\ & \left. + \frac{D(\mu_f)}{\sinh\left(\frac{q}{\mu_f}\right)} \cosh\left(\frac{q}{d_f \mu_f}\right) \right\}. \end{aligned} \quad (28)$$

In this limit, the first term in the square brackets in Eq. (14) is small in comparison with the second one. Thus, one may conclude that the first term in Eq. (14) plays the main role in the dirty limit, while the second term of Eq. (14) describes mainly the clean limit when trajectories of motion are essential.

E. Josephson current

To calculate the Josephson current J of a SIFS ferromagnetic tunnel junction we start from the expression¹

$$\begin{aligned} J &= 4eN(0)v\pi T \sum_{\omega>0} \int_{-1}^1 (\text{Im } g_{11}) \cos\theta d(\cos\theta) = \\ &= 4eN(0)v\pi T \sum_{\omega>0} \int_0^1 (\text{Im } g_{11}^a) \mu d\mu. \end{aligned} \quad (29)$$

Here $N(0)$ is the density of state at the Fermi surface, v is the Fermi velocity, g_{11} is the matrix element of the antisymmetric part of the Eilenberger function that is define by the following expression:

$$\hat{g}^a = \frac{1}{2} \begin{bmatrix} g(\theta) - g(-\theta) & f(\theta) - f(-\theta) \\ f^+(\theta) - f^+(-\theta) & -g(\theta) + g(-\theta) \end{bmatrix}.$$

We apply the tunnel hamiltonian approach and use the boundary conditions on the dielectric interface. These boundary conditions are matching the quasiclassical electron propagators g and f on both sides of the boundary.

The boundary conditions may essentially depend on the quality of the interface. In the case of a nonmagnetic specularly reflecting boundary between two metals these conditions read²⁴

$$\hat{g}^a (R\hat{g}_+^{c2} + \hat{g}_-^{c2}) = D_I \hat{g}_-^c \hat{g}_+^c. \quad (30)$$

$$\hat{g}_1^a = \hat{g}_2^a = \hat{g}^a. \quad (31)$$

Here D_I and $R_I = 1 - D_I$ are the interface transparency and reflectivity coefficients, the index 1(2) labels the functions on the right (left) side from the boundary plane, and the symmetric parts of the quasiclassical Eilenberger functions are defined by the equalities

$$\hat{g}_-^c = \frac{1}{2} (\hat{g}_1^c - \hat{g}_2^c), \quad \hat{g}_+^c = \frac{1}{2} (\hat{g}_1^c + \hat{g}_2^c), \quad (32)$$

$$\hat{g}_{1,2}^c = \frac{1}{2} \begin{pmatrix} g_{1,2}(\theta) + g_{1,2}(-\theta) & f_{1,2}(\theta) + f_{1,2}(-\theta) \\ f_{1,2}^+(\theta) + f_{1,2}^+(-\theta) & -g_{1,2}(\theta) - g_{1,2}(-\theta) \end{pmatrix}.$$

Assuming that the insulating layer transparency is small, $D_I \ll 1$, $R_I \approx 1$, and taking into account that $\hat{g}_1^2 = \hat{g}_1^1 = \hat{1}$, we can expand the boundary conditions (30) in powers of D_I .

For SIFS tunnel structures with s -wave pairing in the electrodes, in this limit it immediately follows that the functions $g_2(\theta) = g_s(\theta)$ and $f_2(\theta) = f_s(\theta)$ are independent on θ and coincide with the expressions for spatially

homogeneous superconducting electrodes

$$f_f = F_f(\theta) \exp\{+i\varphi/2\}, \quad f_s = F_s \exp\{-i\varphi/2\},$$

$$F_s = \frac{\Delta_0}{\sqrt{\omega^2 + \Delta_0^2}}, \quad g_s = \frac{\omega}{\sqrt{\omega^2 + \Delta_0^2}}. \quad (33)$$

Here Δ_0 and φ are the absolute value and the phase difference of the order parameter in the electrodes. The boundary conditions (30) reduce in this case to

$$\hat{g}^a = D_I \hat{g}_-^c \hat{g}_+^c = \frac{D_I}{4} (\hat{g}_1^c \hat{g}_2^c - \hat{g}_2^c \hat{g}_1^c) =$$

$$= \frac{D_I}{4} \begin{pmatrix} f_1 f_2^+ - f_2 f_1^+ & 2(g_1 f_2 - f_1 g_2) \\ 2(f_1^+ g_2 - g_1 f_2^+) & f_1^+ f_2 - f_2^+ f_1 \end{pmatrix}. \quad (34)$$

Then the expression for the Josephson current (29) has the form

$$J = \frac{1}{2} e N(0) v \pi T \sum_{\omega=-\infty}^{\infty} \int_{-\pi/2}^{\pi/2} [f_2^+(\theta) f_1(\theta) -$$

$$- f_2(\theta) f_1^+(\theta)] \cos \theta d(\cos \theta). \quad (35)$$

Using the definition (1) and its symmetry properties (11) and (12), one can find the result for the Josephson current J of the tunnel junction $J = J_C \sin \varphi$, where

$$J_C = \frac{8\pi T}{e R_N} \sum_{\omega>0} \Phi_+(\mu_s) \int_0^1 D_I(\mu_f) \operatorname{Re} [\Phi_+(\mu_f)] \mu_f d\mu_f. \quad (36)$$

The Eilenberger function of the left electrode $\Phi_+(\mu_s)$ is also defined by (8).

The thin insulating layer is considered as a high potential barrier for electrons. The transmission probability is inversely proportional to the exponent of a distance passed by an electron, i.e. $\sim \exp(-d_I/\cos \theta)$, where d_I is the dielectric thickness. Namely, it can be found from the well known expression²⁹ for the transmission coefficient of a square potential barrier of a thickness a , that

$$D_I(a) = \frac{4k_1^2 k_2^2}{4k_1^2 k_2^2 + (k_1^2 + k_2^2)^2 \sinh^2(k_2 a)} \approx$$

$$\approx \frac{4k_1^2 k_2^2}{(k_1^2 + k_2^2)^2} \exp(-2k_2 a), \quad (37)$$

if $k_2 a \gg 1$. Here k_1 and ik_2 are wave vectors of particles outside and inside the barrier. The expressions for the transmission coefficient of the FS boundary (17),(19) were obtained in the same way. Taking into account that $a = d_I/\mu$, one can write the dependence $D_I(\mu)$ in the form

$$D_I(\mu) = \widetilde{D}_0 \exp\left(-\frac{\alpha}{\mu}\right). \quad (38)$$

Here α is a decaying coefficient, that depends on the thickness and material of the insulator. It is useful for a numerical calculation to redefine the value $\widetilde{D}_0 = D_0 \exp(-\alpha)$, and finally

$$D_I(\mu) = D_0 \exp\left(-\alpha \frac{1-\mu}{\mu}\right). \quad (39)$$

III. DISCUSSION

A. Main cases

First, we start from the analysis of the Eilenberger function $\Phi_+(x, \mu_f)$, which describes the superconducting properties of a ferromagnetic Josephson junction. In the simplest case $\Phi_+(x, \mu_f)$ is an exponential function $\Phi_+(x) \propto \exp(x/\xi)$, $x \leq 0$, or a combination of exponential functions, with a complex coherence length^{1,2}

$$\xi^{-1} = \xi_1^{-1} + i\xi_2^{-1}. \quad (40)$$

Here ξ_1 describes the decay of the superconducting correlations at some distance from the FS boundary, while ξ_2 defines the period of LOFF oscillations^{30,31}. For the described FS structure, $\Phi_+(x, \mu_f)$ is given by the expressions (14) and (20)-(22). Now we try to describe the main features of the proximity effect in an FS structure. If the superconducting layer is thick enough to be considered as semi-infinite, and if in-plane nonuniformities connected with sample preparation and the domain structure of the ferromagnetic film can be neglected, the structure has one geometric parameter — the ferromagnet thickness d_f . The properties of the F material give three more characteristic lengths: the electron mean free path in the ferromagnet ℓ_f , the nonmagnetic coherence length ξ_0 , and the characteristic magnetic length ξ_H . The main questions at this stage are: can the Eilenberger function be approximated by an exponential function, and what is the relation between ξ_1, ξ_2 and the characteristic lengths mentioned above.

The Fermi velocity for usual ferromagnetic metals²⁷ is $v_f \sim 3 \cdot 10^7$ cm/s, and if even the temperature $T \sim T_c$, $\xi_0 \sim 100$ nm, i.e. ξ_0 is much larger than other parameters of the problem in usual cases. The value of ξ_0 is difficult to decrease. The gradual increase of ℓ_f leads to the following four cases:

1. $\ell_f \ll \xi_H, d_f$ — the well investigated dirty limit. This condition allows averaging of the Eilenberger functions over trajectories and using the Usadel equations. Φ_+ is given by the expression (24), and for a strong exchange field ($H \gg k_B T_c$), $\xi_1 = \xi_2 = \sqrt{2\ell_f \xi_H/3}$.

2. $\ell_f \sim \xi_H, d_f$ — the intermediate case. The Usadel equations cannot be used, and one needs to solve the Eilenberger equations taking into account the $\Phi_+(\theta)$ dependence. Up to now the linearized equations were solved only for an SFS junction^{4,5}, and the obtained expressions are so complicated that they are very difficult to analyze. This is the most interesting case for our analysis, which allows to find out when this case reduces to the dirty limit and under which conditions the Usadel equations are applicable.

3. $\xi_H \ll \ell_f < d_f, \xi_0$ — the clean limit. Here, $\Phi_+(x, \theta)$ is defined mainly by the second term of Eq. (14), and^{4,32} $\xi_1 \sim \ell_f, \xi_2 \approx \xi_H$.

4. $\ell_f \gg d_f$ — the ballistic regime cannot be considered within the framework of our approach, excluding the case

$\xi_1 \ll d_f$ when multiple reflections from the interfaces can also be neglected. The ballistic SFS junction was considered earlier^{5,18,25,33-35}, and the dependence $J_C(d_f)$ cannot be presented as an exponent in the general case²⁵.

B. Analysis of cases 1-3

In all plots presented below we use the same normalization for all lengths: $x, d_f, l_f, \xi_0, \xi_H, \xi_1, \xi_2$. All of them are normalized to some unit length Ξ , which, in fact, can be chosen arbitrarily, e.g. $\Xi = 1$ nm. Note that only the ratios between the lengths given above are important, i.e., if one divides the above list of lengths by any arbitrary constant Ξ all the results remain unchanged. For example, in all plots we use $\xi_0 = 81$.

a. Influence of different types of FS boundary transparency. Figure 1 shows the spatial distribution of the functions $\langle \Phi_+(x) \rangle$ calculated from (4) for $l_f = 7$, $\xi_H = 3$, $d_f = 10$ and $J_C(d_f)$ calculated from (36) for $l_f = 7$, $\xi_H = 3$, and the insulating layer decay parameter $\alpha = 5$. It is clearly seen that the angular dependence of SF interface transparency influences both, the amplitude and period of oscillations of the presented curves. For the particular choice of parameters this influence can be easily explained.

For the case of a transparency which is independent on μ_f , the Eilenberger functions are initiated from the SF interface in all directions, thus leading to the largest amplitude of $\langle \Phi_+(x) \rangle$ oscillations. Simultaneously, the contributions to $\langle \Phi_+(x) \rangle$ coming from rapidly decaying Eilenberger functions with a large argument θ_f result in the appearance of the smallest period of $\langle \Phi_+(x) \rangle$ oscillations. The stronger the angular dependence of the SF interface transparency coefficient, the smaller are the contributions to average values from the rapidly decaying Eilenberger functions, and as the result the larger is the period and the smaller is the amplitude of $\langle \Phi_+(x) \rangle$ oscillations. It is necessary also to mention that $\langle \Phi_+(x) \rangle$ decays more rapidly with $|x|$ than $\Phi_+(x, 1)$. This difference is the smaller the smaller is l_f .

From (36) it follows that in general the contribution to the junction critical current comes not only from $\Phi_+(x, 1)$, but also from $\Phi_+(x, \mu_f)$ located in a narrow domain of μ_f nearby $\mu_f = 1$. Due to that, the $J_C(d_f)$ curve appears to be sensitive against the angular dependence of the SF interface transparency. We see that the stronger this dependence the smaller is the amplitude of oscillations and the larger are the distances of the 0 to π transition points in $J_C(d_f)$ from the SF interface, while the period of $J_C(d_f)$ oscillations is practically insensitive against the form of $D(\mu_f)$ and coincides with that of $\Phi_+(x, 1)$. If the ferromagnetic layer is thick enough, the sum over ω in (36) converges rapidly, and the main contribution is given by the first term of the sum, which is determined by the real part of the Eilenberger function $\Phi_+(x, 1)$. For these reasons we will focus below on the examination of the properties of the real part of the Eilen-

berger function $\Phi_+(x, 1)$, and in further calculations we will also use the form $D(\mu_f) = D_2\mu_f$ for the transmission coefficient of the FS interface, as it is most applicable to materials used in experiments.

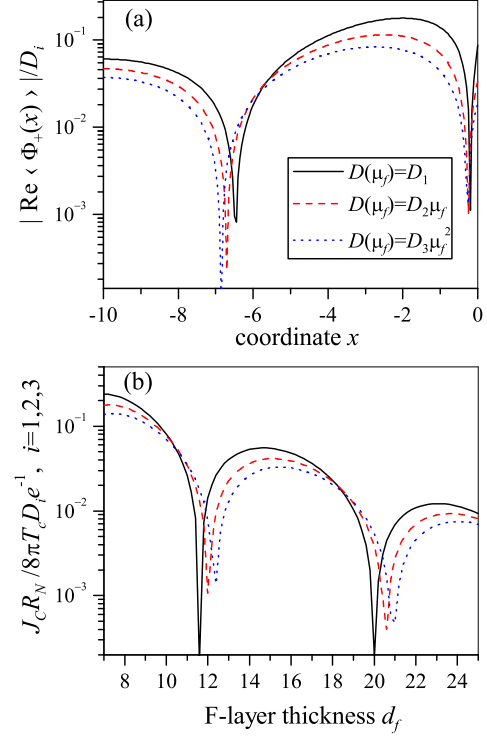


FIG. 1: (Color online) (a) Averaged Eilenberger function $\langle \Phi_+(x) \rangle$ and (b) $J_C(d_f)R_N$ product for different types of the FS interface (16)-(19). The F-layer parameters are $l_f = 7$, $\xi_H = 3$ (a,b), $d_f = 10$ (a), the insulating layer parameter is $\alpha = 5$ (b); $T \approx 0.5T_c$.

b. Spatial profile of the Eilenberger function. The direct comparison (see Fig. 2) of the results of numerical calculations of the real part of the Eilenberger function $\Phi_+(x, 1)$, making use of Eq. (21), with the curves which follow from the simple analytical expression

$$\Phi_+^{app}(x, 1) \approx \frac{\Phi_+(0, 1)}{\cosh(d_f/\xi)} \cosh \frac{x + d_f}{\xi} \quad (41)$$

confirms that it is possible to approximate $\Phi_+(x, 1)$ by this simple formula. It satisfies the boundary condition on the dielectric interface (9) and contains the factor $\Phi_+(0, 1)$, which has been calculated numerically from (21).

The quality of the approximation (41) was checked for different values of parameters for all dependencies investigated further. It was found to be satisfactory in the whole accessible range of parameters $d_f > l_f$ or ξ_1 . This approximation yields the values of ξ , i.e. ξ_1 and ξ_2 .

c. Dependence of ξ on the junction parameters. The attempt to find ξ in the area of intermediate scattering was made earlier³⁶. It was supposed in Ref. [36] that ξ

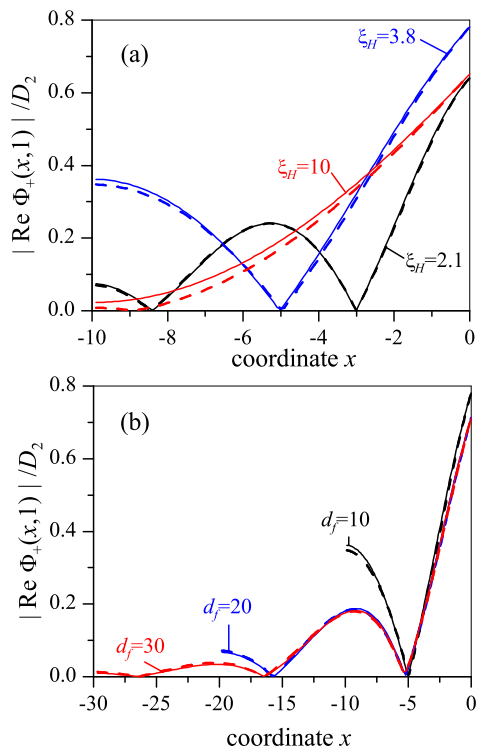


FIG. 2: (Color online) The exact $\Phi_+(x, 1)$ (solid lines) and approximated $\Phi_+(x, 1)^{app}$ (dashed lines) Eilenberger function (a) for different values of ξ_H corresponding to a local maximum, minimum, and smooth region of the dependence $\xi_1(\xi_H)$; see Fig.3(b), at $\ell_f = 7$, $d_f = 10$; (b) for different thicknesses d_f at $\ell_f = 7$, $\xi_H = 3.8$. $T \approx 0.5T_c$.

may be found as a solution of the equation

$$i\ell_f/\xi = \arctan(i\ell_f/k_f\xi), \quad (42)$$

which determines the poles of the sum in Eqs.(14), (15) for $\Phi_+(x)$ and $\langle \Phi_+(x) \rangle$, respectively. Unfortunately, the inverse tangent is a multivalent function. In the general case this fact prevents to represent $\Phi_+(x)$ and $\langle \Phi_+(x) \rangle$ as only the sum of residues of summable functions in (14), (15). An exception occurs in the range of parameters for which the ferromagnet is close to the dirty limit. In this case the sum in (14) and (15) converts faster than the multivalent nature of the inverse tangent becomes essential. These difficulties had been first pointed out in Ref. [37], where it was also demonstrated that the solution of the Eilenberger equations used in Ref. [36] does not transfer correctly to the solution of the Eilenberger equations in the clean limit.

To avoid these mathematical difficulties we have decided to find out the dependence $\xi(\xi_H, \ell_f)$ from the direct fitting of the real part of $\Phi_+(x)$ calculated numerically from (14) by approximating formula (41). The result of this procedure is demonstrated in Fig. 3. It shows the dependencies of ξ_1 and ξ_2 on the magnetic length ξ_H at different ℓ_f . The solutions from Ref. [36] are also pre-

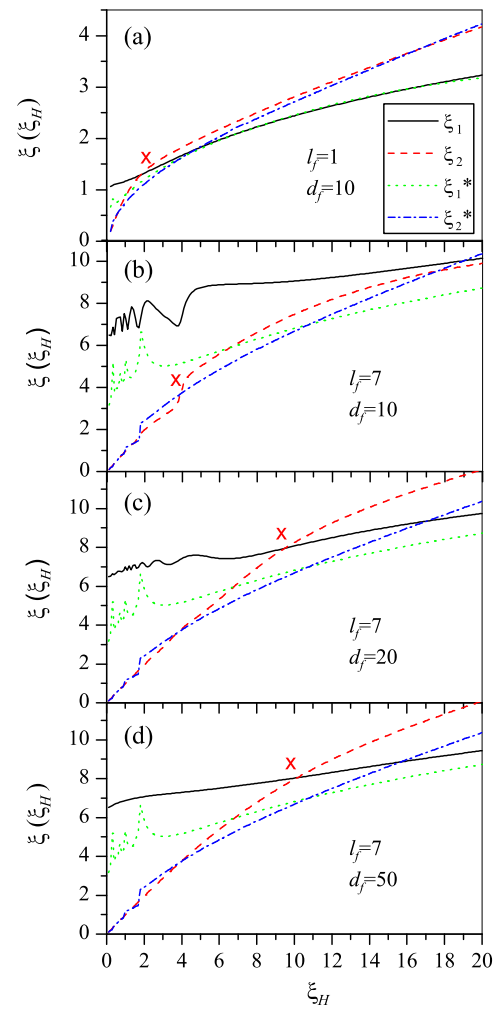


FIG. 3: (Color online) Decay length ξ_1 and oscillation parameter ξ_2 vs magnetic length ξ_H for different values of ℓ_f and d_f , that are denoted in the plots. The corresponding values of ξ from Ref. [36] are also shown and marked by *.

sented in Fig. 3 for comparison. They coincide with our values when $\xi_H \gg \ell_f$ i.e. in the dirty limit. We have taken two cases for the numerical investigation: $\ell_f = 1$, that is close to the dirty limit, and $\ell_f = 7$, that is close to the clean case.

It is seen, that ξ_1 oscillates with the exchange energy H (so as $\xi_H \sim H^{-1}$), an interesting result, that was not noted earlier. These oscillations appear in rather clean samples $\ell_f \gtrsim d_f/\pi$ and for $\xi_H < d_f/\pi$. They originate mainly from the second term of the expression (14), which plays the main role in the clean case. The function $\xi(\xi_H)$ changes with increasing d_f (cf. Fig. 3(b-d)). At large enough d_f , electrons have a time to scatter in the ferromagnet, their trajectories shuffle, and the dominant role of the "clean" term vanishes, the oscillations disappear, see Fig. 3(d). We note that the smaller is the probability of dephasing of the Eilenberger functions due to electron scattering in the F layer, the stronger are

the interference effects between the IF and FS interfaces. This interference demands, for given values of ξ_1 and ξ_2 , the fulfillment of the boundary conditions at these interfaces, which fix the value of the phase derivatives at $x = 0$ and $x = d_f$. As it follows from Eq. (20)-(22), these conditions cannot be satisfied on the class of monotonic ξ_1 and ξ_2 functions. Therefore the transition from the dirty to the clean limit should be accompanied by a non-monotonic behavior of ξ_1 and ξ_2 as a function of ξ_H for fixed ℓ , see Fig. 3, or as a function of ℓ for fixed ξ_H , see Fig. 4.

In the dirty limit the spatial oscillation length $\xi_2 \approx \sqrt{2\ell_f \xi_H}/3$, while in the clean limit $\xi_2 \approx \xi_H$. Near the point marked by X in Fig. 3 there is a crossover between the dependencies corresponding to dirty and clean limits, respectively, i.e. this region can be considered as a boundary between the clean and the dirty cases.

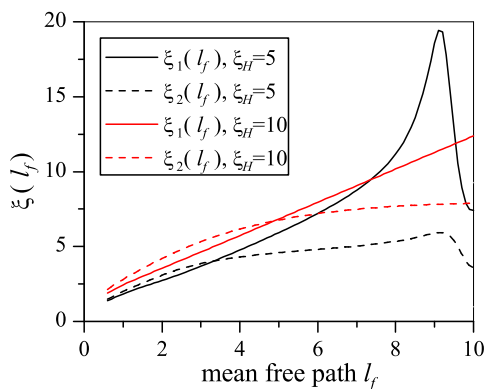


FIG. 4: (Color online) Decay length ξ_1 (solid lines) and oscillation parameter ξ_2 (dashed lines) vs electron mean free path ℓ_f in the ferromagnet for different values of ξ_H ; here $d_f = 10$, $T \approx 0.5T_c$.

The dependence of ξ on the mean free path ℓ for different ξ_H is presented in Fig. 4. Usually the decay length ξ_1 as well as the oscillation period $2\pi\xi_2$ increase with the mean free path, which corresponds to the results in Ref. [5]. However, the dependence $\xi(\ell_f)$ may be non-monotonic for some values of the ferromagnet thickness.

In the presented figures one can see, that ξ_1 may be larger or smaller than ξ_2 and may behave nonmonotonically. This depends not only on the material constants of ferromagnetic material, but also on the thickness of the F layer.

The found values ξ_1 and ξ_2 together with the simple dependence (41) could be widely used for various estimations, approximate calculations, and fitting experimental data, for example for a measurement of the density of states (DOS) in an FS bilayer or calculation of thickness dependence of the critical current of SIFS Josephson junctions.

d. $J_C(d_f)$ in the limit of large d_f . As an example, we consider the critical current of SIFS Josephson junctions in the limit of large F layer thickness $d_f \gg \xi_1$. In

this limit the main contribution to the critical current in (36) is given by the term at $\omega = \pi T$. Suppose further that only electrons, that are incident in the direction perpendicular to the FI interface, provide the current across it, from (36), (41) we have

$$J_C = \frac{8\pi T D_2}{e R_N} \operatorname{Re} \frac{\Delta_0 \Phi_+(0, 1)}{\sqrt{(\pi T)^2 + \Delta_0^2} \cosh(d_f/\xi)} \quad (43)$$

The comparison with the exact numerical calculation has shown that this expression (43) well approximates $J_C(d_f)$ starting from $d_f \gtrsim \xi_1$. The thickness dependence of J_C calculated from (43) at the value ξ taken at $d_f = 50$, see Fig.3(d), for $\ell_f = 7$, $\xi_H = 2.1$, $T \approx 0.5T_c$ is shown in Fig. 5 by the solid line. The dashed and dashed dotted curves in Fig. 5 give the results obtained by numerical calculation, which have been done for the same parameters with the use of the exact expression for $\Phi_+(-d_f, \mu_f)$ in (36) and at different insulating layer thicknesses described by the parameter α .

It is clearly seen that the larger is α the closer is the result to the approximation formula (43). We may also conclude that the difference between the asymptotic solid curve and the dashed curves in Fig. 5 calculated for finite values of α occurs only in amplitude and positions of the 0 to π transition points, while the decay length and period of $J_C(d_f)$ oscillations are nearly the same. This means, that if in experiment we are mainly interested in the estimation of the ferromagnet material constant, ξ , we may really use for the data interpretation the simple expression (43) and consider the coefficient $\Phi_+(0, 1)$ in it as a phenomenological parameter, which depends not only on the properties of ferromagnetic material, but also on d_f in a rather complicated way, see Fig.2(b), as well as on the form of the transparency coefficients at the FI and FS interfaces. Although our results for SIFS junctions give the same ξ_1 and ξ_2 as for SFS junctions (at least for a thick F layer), different boundary conditions result in different order parameter amplitude and phase. This results in a different $J_C(d_f)$ dependence, similar to the results obtained earlier in dirty limit³⁸.

It is interesting to note that in the case of a rather thin insulating barrier and rather clean ferromagnet, ξ_1 and ξ_2 as measured from the critical current of SIFS junctions may differ from ξ as measured from the DOS on the free F surface of an analogous FS bilayer. This is because the DOS measured by low-temperature scanning tunneling spectroscopy (which may only yield contributions from electrons with normal incidence) is directly given by $\Phi_+(-d_f, \mu_f = 1)$, while J_C includes contributions from other angles.

e. Applicability of the Usadel equation. The condition that allows using the Usadel equation is well known — this is strong nonmagnetic scattering¹⁶, namely, $\ell_f \ll \xi_H, d_f, \xi_0$. What does the symbol “ \ll ” mean exactly? In order to illustrate this, Fig. 6 shows the dependence $J_C(\ell_f)$ given by the expression (21). Two parts of (21), called for convenience “dirty” and “clean”, are given by the first and the second terms of the expression (21). The

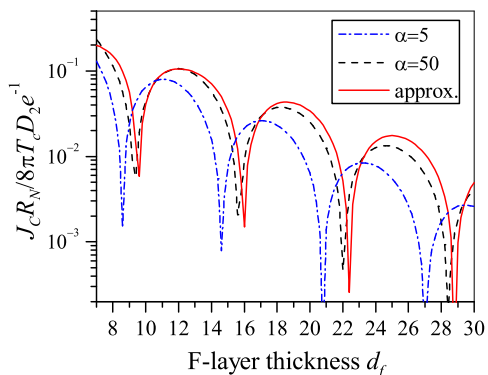


FIG. 5: (Color online) $J_C R_N$ product as a function of the ferromagnet thickness d_f at different insulating layer thicknesses described by the parameter α , and the approximation by expressions (36),(41) at the value ξ taken at $d_f = 50$, see Fig.3(d), here $l_f = 7$, $\xi_H = 2.1$, $T \approx 0.5T_c$.

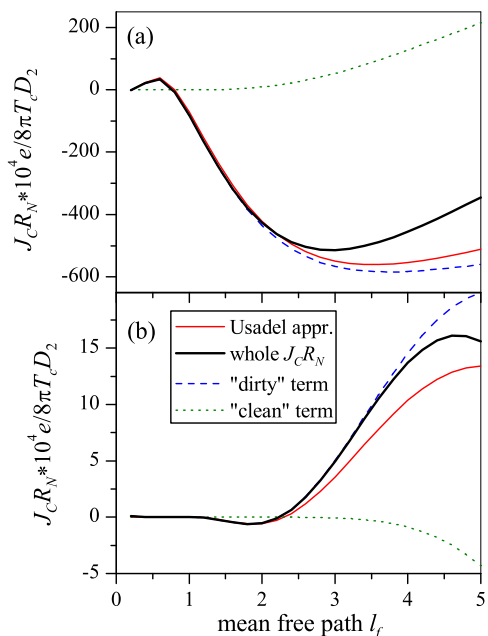


FIG. 6: (Color online) $J_C R_N$ product vs ferromagnet mean free path l_f ($\xi_H = 10$, $T \approx 0.5T_c$, $\alpha = 5$) for $d_f = 10$ (a) and $d_f = 30$ (b). Each plot shows $J_C R_N$ obtained from the Usadel function (15), from the Eilenberger function Φ_+ (21), as well as from only the first "dirty" term or only the second "clean" term of (21).

critical current density as given by the Usadel function (27), describing the dirty limit, is also shown. $J_C(l_f)$ coincides with the Usadel solution at $l_f \approx 0.1\xi_H$, then the first term in square brackets in Eq. (21) dominates and the μ_f -dependence becomes nonsignificant due to the spatial averaging as a result of multiple scattering. This means, that the Usadel equations become appropriate to use if the parameter $H\tau_f \leq 0.1$. This result was

intuitively clear, but demanded a proof due to plenty of investigations, where the Usadel equations was used at $H\tau_f \lesssim 1$.

IV. COMPARISON WITH EXPERIMENT

There are only few experiments on SIFS tunnel junctions with moderate scattering in the F-layer^{10,39}. In Ref. [10] experimental data points for $J_C(d_f)$ are rather sparse, while in Ref. [39] the density of data points per period is much larger. We thus decided to compare our theory to the data of Ref. [39].

This article³⁹ also contains attempts to fit the experimental data by theoretical curves, however, without much success. Some of these attempts, see Fig.5(a) in Ref. [39], use a theory developed for a very clean (ballistic) SFS junction. The predicted oscillation period of $J_C(d_f)$ was significantly smaller than the one in the experiment. Figure 5(b) in Ref. [39] shows the same experimental data together with fits using dirty limit theory. The best fit was achieved with $\xi_1 = 0.66$ nm and $\xi_2 = 0.53$ nm. However, the theory for a dirty ferromagnetic junction cannot explain $\xi_1 > \xi_2$, and all of these theories, both clean and dirty, do not take into account the insulating layer.

In Ref. [39] and Ref. [40] it was found, that the magnetic anisotropy of the F layer changes from perpendicular to in-plane with an increase of the F-layer thickness. Perpendicular magnetic anisotropy in a polycrystalline thin film may occur due to several reasons: the mechanism described by Neel⁴¹ related to the absence of nearest neighbor F-layer atoms near interfaces, the magnetostriction mechanism, the surface roughness, and the one associated with microscopic-shape anisotropy⁴². The latter may also vary for samples sputtered under different angles⁴². Perpendicular magnetic anisotropy can change to an in-plane anisotropy due to a competition with the shape anisotropy of a film. However, none of the mechanisms listed above can be expected to give a significant jump of the exchange magnetic energy H at the transition between the two types of anisotropy. There is some shift of the experimental curve, see Fig.2(a) in Ref. [39], at $d_f = 3.8$ nm, where the anisotropy changes. But there are no reasons to assume, that this change of anisotropy is associated with a significant change of H . Therefore, we try to describe the whole experimental curve $J_C(d_f)$ using the same value of H .

The common problem for all explanations of this experiment is the location of the first minimum of $J_C(d_f)$ at a rather large $d_f \approx 3$ nm in comparison with the oscillation length $\xi_2 \approx 0.5$ nm. The authors³⁹ attribute this to the existence of a nonmagnetic dead layer with rather large thickness $d_{dead} = 2.26$ nm in the Ni layer.

We note, that d_{dead} , in general, depends on d_f . We assume that $d_{dead} = d_f$ up to some value d_{max} and then either d_{dead} stays constant at a saturation value $d_{dead}^{sat} = d_{max}$ with further increase of d_f , or it is reduced

to a constant value $d_{dead}^{sat} < d_{max}$. For the latter case there are the following reasons. The dead layer may consist of a nonmagnetic Ni alloy with magnetic clusters or islands, which are not connected by the exchange interaction. A very thin film of a ferromagnetic material may be paramagnetic. When one covers it by extra magnetic layers, some part of its thickness may magnetize. First, magnetic clusters uncoupled by the exchange interaction can couple if they are covered by extra magnetic layers. Second, a thin homogeneous film of a magnetic material of the thickness of a few monolayers exhibits nonmagnetic properties alone, but becomes magnetic entirely when its thickness increases, due to the transition from the two-dimensional to the three-dimensional case.

The dead layer is described as a normal layer, that yields $J_C(d_f) \sim \exp(-\frac{d_f}{\xi_N})$. The best fitting presented in Fig. 7(a),(b) by straight short-dashed lines, gives the value³⁹ $\xi_N = 0.68$ nm. The normal metal coherence length ξ_N depends both on the nonmagnetic and paramagnetic scattering. The latter may be significant in the dead layer in the presence of many magnetic inhomogeneities (clusters and impurities). Following a theory developed for SFS junctions⁷ taking into account magnetic scattering, one can find the expression for the coherence length of a normal metal (at $H = 0$) with magnetic impurities $\xi_N = \sqrt{\frac{D_f}{2(\pi T + 1/\tau_m)}}$, where τ_m is the magnetic scattering time. We assume that the mean free path has the same value as in the rest of the magnetic Ni layer, $\ell_f = 0.6$ nm, that is given by the fit. This yields $\tau_m = 1.68 \cdot 10^{-14}$ s. For comparison, the nonmagnetic scattering time is found to be almost 8 times less. Fig. 7(a),(b) shows that the obtained value of ξ_N is very close to the decay length of the magnetic SIFS junction at $d_f > d_{max}$. In the absence of the exchange field its pair-breaking role is played by the magnetic scattering in this structure.

We consider two possibilities to explain the experimental data³⁹. First, we assume that the detected minimum of $J_C(d_f)$ is the first one, see Fig. 7(a). Treating the dead layer as a normal layer ($H = 0$), our best fit yields $d_{dead}^{sat} = d_{max} = 2.37$ nm. The fitting yields the following values of the F-layer parameters: $\ell_f = 0.6$ nm and $\xi_H = 0.6$ nm, that corresponds to $H = 1782$ K or $H = 154$ meV.

As a second scenario we assume that the detected minimum of $J_C(d_f)$ is the second one, see Fig. 7(b). The first $J_C(d_f)$ minimum may not show up if the effective thickness of the dead layer *decreases* as soon as d_f is above the threshold value d_{max} . Then, at the value of d_f where $J_C(d_f)$ is supposed to have the first minimum, the F layer may still be nonmagnetic, while at large values of d_f it has some small value d_{dead}^{sat} . For that scenario $d_{dead}^{sat} = 0.2$ nm provides the best fit. The mean free path was found as $\ell_f = 0.6$ nm, $\xi_H = 0.956$ nm, that corresponds to $H = 1119$ K or $H = 96.4$ meV.

In both fits we used the following parameters. The temperature $T = 4.2$ K and $T_c = 8$ K were taken like

in the experiment³⁹, that yields $\xi_0 = 81$ nm. Fermi velocities²⁷ $v_f = 2.8 \cdot 10^7$ cm/s and²⁶ $v_s = 6.2 \cdot 10^7$ cm/s were taken. Since $v_s > v_f$, we use the FS boundary condition in the form (17). The thickness of the insulating Al_2O_3 barrier was not measured exactly; still the value $\alpha = 5$ seems to be realistic, see Eq.(39). The values of the exchange field for both cases are within the range obtained for Ni in SFS experiments^{8,14,15,27}. The relation $\ell_f \sim \xi_H$ does not allow using the Usadel equations, however, this is not far from the dirty limit.

Comparing both fits shown in Fig. 7(a),(b) we cannot give a definite answer which minimum (the first or the second) was observed in the experiment³⁹, but we are able to explain the fact that $\xi_1 > \xi_2$ in any case. Such relation between ξ_1 and ξ_2 cannot be obtained from a dirty limit theory.

The Josephson junctions used in the experiment³⁹ contain an extra normal layer of Cu between the I and F layer. A normal layer cannot change ξ , which mainly depends on properties of the magnetic layer. However, it may change the boundary conditions. Therefore, our theory cannot be directly applied for the determination of the exact value of the dead layer, but may explain the obtained value of ξ .

For the analysis of the first minimum position and the dead layer estimation we may also use the theory developed earlier for the dirty limit, since the estimated value of $\ell_f \sim \xi_2$. From the analysis of the uniform part of the solutions obtained in Ref. [43] for dirty SINFS and SIFNS junctions, it follows that the first minimum of the $J_C(d_f)$ dependence must be at $(d_f - d_{dead})/\xi_2 \approx 3\pi/4$. If we assume that the detected minimum of $J_C(d_f)$ is the first one, then, the estimation yields $d_{dead}^{sat} = d_{max} = 1.8$ nm. This value is rather large (it is larger than the oscillations halfperiod), similar to Ref. [39]. If we assume that the detected minimum of $J_C(d_f)$ is the second one, then the first one must be located at $d_f \approx 1.4$ nm and the dead layer thickness $d_{dead}^{sat} = 0.2$ nm. There is a small shift of experimental data for $J_C(d_f)$ at the thickness $d_f \approx 1.4$ nm, but a real $0-\pi$ transition was not detected, possibly, due to the fact that $d_{dead}^{sat} < d_{max}$. Generally speaking, if we assume that $d_{dead}(d_f)$ jumps from d_{max} to d_{dead}^{sat} at d_{max} then one should see a jump on $I_C(d_f)$ dependence. However in our case it not observed, see Fig.7(a) and (b). We suppose that this is related to the fact that $\xi_N \approx \xi_1$.

Figure 7(c) contains also calculated curves, plotted for the same model parameters as in Fig. 7(b) but for a cleaner ferromagnet. Usually the purpose of the experimental investigations of SIFS structures is the design of a π -Josephson junction with a large $J_C R_N$. R_N is determined mainly by the insulating barrier. Our calculations show that by increasing ℓ_f one can increase J_C by 1-2 orders of magnitude, see Fig.7(c). It would also be reasonable to delete extra normal layers to achieve the π -phase at a smaller d_f , and consequently, to have larger J_C ; see also Refs. [38,44].

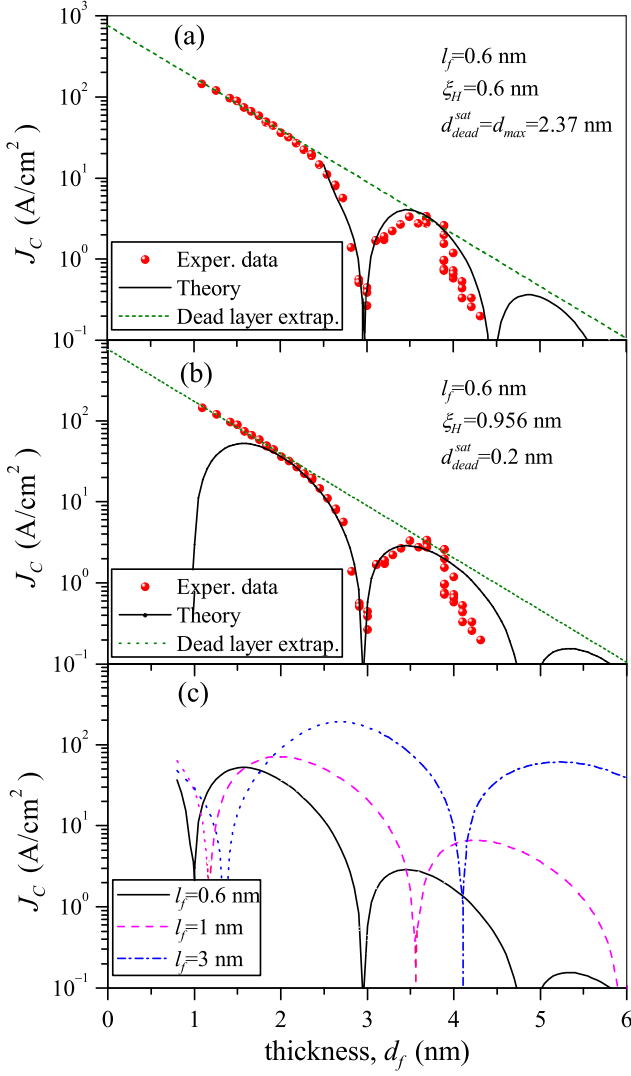


FIG. 7: (Color online) (a) and (b) show a comparison of $J_C(d_f)$ from the presented theory with experiment³⁹. Dashed lines are fits to the experimental data in the range $d_f < 2.37$ nm, where the F layer can be interpreted as nonmagnetic. (c) Dependencies $J_C(d_f)$ at lower scattering. Parameters are like in (b). The regime for which multiple reflections cannot be neglected are marked by dotted lines.

V. CONCLUSION

The SIFS ferromagnetic tunnel Josephson junction has been investigated within the framework of the quasiclassical Eilenberger equations, that allow a description of both, the clean and the dirty limits, as well as an arbitrary scattering. The Eilenberger function $\Phi_+(x, \mu_f)$ may be approximated by the simple formula (41) within the entire range of considered parameters. The decay length ξ_1 and the oscillation period $2\pi\xi_2$ depends not only on the mean free path ℓ_f and the exchange energy H in the ferromagnet, but also on the ferromagnet thick-

ness d_f , and can be nonmonotonic as a function of ξ_H or ℓ_f .

The approximation of $J_C(d_f)$ by an exponential function or its combinations has some restrictions. The applicability of the Usadel equation has been established for $\ell_f \lesssim 0.1\xi_H$.

The developed approach has been used to fit experimental data³⁹ providing a satisfactory fitting of the $J_C(d_f)$ dependence. It allows to explain the values $\xi_1 > \xi_2$ and to give some practical recommendations on how to increase the $J_C R_N$ product.

Acknowledgments

We gratefully acknowledge M. Weides for providing experimental data and helpful discussions, as well as A.B. Granovskiy and N.S. Perov. This work was supported by the Russian Foundation for Basic Research (Grants 10-02-90014-Bel-a, 10-02-00569-a, 11-02-12065-ofi-m), by the Deutsche Forschungsgemeinschaft (DFG) via the SFB/TRR 21 and by project Go-1106/03, by the Deutscher Akademischer Austauschdienst.

Appendix A

Substituting the expression (13) into the Eilenberger equation (6), multiplying the obtained equations by $\cos[\pi k(x + d_f)/d_f]$, and integrating them over x one can find the relation between coefficients Q_m and B (10), namely

$$Q_m = \frac{\langle Q_m \rangle + \left\langle B \frac{\zeta_f}{d_f} \frac{(-1)^m}{M} \sinh \frac{d_f}{\zeta_f} \right\rangle}{k_f M}, \quad (\text{A1})$$

where

$$M = \pi^2 m^2 \frac{\mu_f^2}{q^2} + 1, \quad \left\langle \frac{1}{M} \right\rangle = \frac{q}{\pi m} \arctan \frac{\pi m}{q}.$$

Averaging both sides of (A1) over the angle θ we get

$$\langle Q_m \rangle = \left\langle B \frac{\zeta_f}{d_f} \frac{(-1)^m}{M} \sinh \frac{d_f}{\zeta_f} \right\rangle \frac{\left\langle \frac{1}{k_f M} \right\rangle}{\left[1 - \left\langle \frac{1}{k_f M} \right\rangle \right]}. \quad (\text{A2})$$

A substitution of (A2) into (A1) finally gives the relation between the coefficients in expression (13).

$$Q_m = \frac{\left\langle B \frac{\zeta_f}{d_f} \frac{(-1)^m}{M} \sinh \frac{d_f}{\zeta_f} \right\rangle}{M} \frac{1}{\left[k_f - \left\langle \frac{1}{M} \right\rangle \right]}. \quad (\text{A3})$$

Expressions (A3) and (13) permit to rewrite the solution of the Eilenberger equations in the closed form

$$\Phi_+ = \sum_{m=-\infty}^{\infty} \frac{\left\langle B(\mu) \frac{(-1)^m \mu}{M(\mu)} \frac{\sinh \frac{q}{\mu}}{\mu} \right\rangle_{\mu}}{M(\mu_f) \left[k_f - \left\langle \frac{1}{M} \right\rangle \right]} \cos \frac{\pi m(x + d_f)}{d_f} + B(\mu_f) \cosh \left(q \frac{x + d_f}{d_f \mu_f} \right), \quad (\text{A4})$$

and for an isotropic component $\langle \Phi_+ \rangle$ of this solution to get

$$\langle \Phi_+ \rangle = k_f \sum_{m=-\infty}^{\infty} \frac{\left\langle B(\mu) \frac{(-1)^m \mu}{M(\mu)} \frac{\sinh \frac{q}{\mu}}{\mu} \right\rangle_{\mu}}{\left[k_f - \left\langle \frac{1}{M} \right\rangle \right]} \cos \frac{\pi m(x + d_f)}{d_f}. \quad (\text{A5})$$

The form of the solution of the Eilenberger equations in the S layer essentially depends on transport properties of the FS interface.

If the transparency $D(\mu_f)$ is small, then in the first approximation on $D(\mu_f)$, we can neglect the suppression of superconductivity in the S region and consider the order parameter and the Eilenberger functions as constants independent on space coordinates, which are equal to their bulk values, thus leading to the boundary condition for determination of integration constants $B(\mu_f)$ in the form of Eq. (10). From the boundary condition (10) we get

$$B(\mu_f) = D(\mu_f) \frac{\Delta_0}{\sqrt{\Delta_0^2 + \omega_f^2}} \frac{1}{\sinh \left(\frac{q}{\mu_f} \right)}, \quad (\text{A6})$$

and obtain the analytical solution in the form (14) that, from our point of view, is more convenient for the further analysis than solutions previously used in Refs. [4,5].

For the described three forms (16)–(19) of $D(\mu_f)$ dependencies we get

$$\left\langle D(\mu) \frac{\mu}{M(\mu)} \right\rangle_{\mu} = D_1 \int_0^1 \frac{\mu d\mu}{\pi^2 m^2 \mu^2 / q^2 + 1} = \frac{D_1}{2} \frac{q^2}{\pi^2 m^2} \ln \left(\frac{\pi^2 m^2}{q^2} + 1 \right), \quad (\text{A7})$$

$$\left\langle D(\mu) \frac{\mu}{M(\mu)} \right\rangle_{\mu} = D_2 \int_0^1 \frac{\mu^2 d\mu}{\pi^2 m^2 \mu^2 / q^2 + 1} = D_2 \frac{q^2}{\pi^2 m^2} \left(1 - \frac{q}{\pi m} \arctan \frac{\pi m}{q} \right), \quad (\text{A8})$$

$$\left\langle D(\mu) \frac{\mu}{M(\mu)} \right\rangle_{\mu} = D_3 \int_0^1 \frac{\mu^3 d\mu}{\pi^2 m^2 \mu^2 / q^2 + 1} = \frac{D_3}{2} \frac{q^2}{\pi^2 m^2} \left[1 - \frac{q^2}{\pi^2 m^2} \ln \left(\frac{\pi^2 m^2}{q^2} + 1 \right) \right]. \quad (\text{A9})$$

(A10)

Substituting the averages (A7)–(A9) into the expression (14) we get the Eilenberger function for different FS interface transparencies (20)–(22). The functions (20)–(22) averaged over the angle have the following forms.

First, for $D(\mu_f) = D_1$

$$\langle \Phi_+ \rangle = \frac{\Delta_0 D_1}{\sqrt{\Delta_0^2 + \omega^2}} \left[\frac{1}{2q(k_f - 1)} + \sum_{m=1}^{\infty} \frac{\frac{q}{2\pi^2 m^2} \ln \left(\frac{\pi^2 m^2}{q^2} + 1 \right)}{k_f - \frac{q}{\pi m} \arctan \frac{\pi m}{q}} \cos \frac{\pi m x}{d_f} \right]. \quad (\text{A11})$$

Second, for $D(\mu_f) = \mu D_2$

$$\langle \Phi_+ \rangle = \frac{\Delta_0 D_2}{\sqrt{\Delta_0^2 + \omega^2}} \left[\frac{1}{3q(k_f - 1)} + 2 \sum_{m=1}^{\infty} \frac{\frac{q}{\pi^2 m^2} \left(1 - \frac{q}{\pi m} \arctan \frac{\pi m}{q} \right)}{k_f - \frac{q}{\pi m} \arctan \frac{\pi m}{q}} \cos \frac{\pi m x}{d_f} \right]. \quad (\text{A12})$$

Third, for $D(\mu_f) = \mu^2 D_3$

$$\langle \Phi_+ \rangle = \frac{\Delta_0 D_3}{\sqrt{\Delta_0^2 + \omega^2}} \left[\frac{1}{4q(k_f - 1)} + \sum_{m=1}^{\infty} \frac{\frac{q}{\pi^2 m^2} \left[1 - \frac{q^2}{\pi^2 m^2} \ln \left(\frac{\pi^2 m^2}{q^2} + 1 \right) \right]}{k_f - \frac{q}{\pi m} \arctan \frac{\pi m}{q}} \cos \frac{\pi m x}{d_f} \right]. \quad (\text{A13})$$

Our calculation yields the following value of the suppression parameter for the Usadel equation: $\gamma_B =$

$\ell_f \langle \mu D(\mu) \rangle^{-1} / 3 \sqrt{d_f / 2\pi T_c}$. It differs from the one ob-

tained early²⁸ by a factor 2. We suppose, that this is a consequence of an approximation we have made in boundary conditions (10) at the FS interface. We have neglected all spatial variations in the S part as well as the back influence of the ferromagnet on the superconductor, and this factor 2 is the price for this approximation. If we use the boundary condition (10) in its full form²⁴, we get for γ_B :

$$\gamma_B = \frac{2}{3} \frac{\ell_f}{\sqrt{\frac{d_f}{2\pi T_c}}} \langle \mu D(\mu) \rangle^{-1}.$$

Our three models of the FS interface yield

$$\gamma_B = \frac{2}{3} \frac{\ell_f}{D_1 \sqrt{\frac{d_f}{2\pi T_c}}} \langle \mu \rangle^{-1} = \frac{4}{3} \frac{\ell_f}{D_1 \sqrt{\frac{d_f}{2\pi T_c}}}, \quad (\text{A14})$$

$$\gamma_B = \frac{2}{3} \frac{\ell_f}{D_2 \sqrt{\frac{d_f}{2\pi T_c}}} \langle \mu^2 \rangle^{-1} = 2 \frac{\ell_f}{D_2 \sqrt{\frac{d_f}{2\pi T_c}}}, \quad (\text{A15})$$

$$\gamma_B = \frac{2}{3} \frac{\ell_f}{D_3 \sqrt{\frac{d_f}{2\pi T_c}}} \langle \mu^3 \rangle^{-1} = \frac{8}{3} \frac{\ell_f}{D_3 \sqrt{\frac{d_f}{2\pi T_c}}}. \quad (\text{A16})$$

-
- * Electronic address: pugach@magn.ru
- ¹ A. Golubov, M. Kupriyanov, and E. Il'ichev, Rev. Mod. Phys. **76**, 411 (2004).
 - ² A. I. Buzdin, Rev. Mod. Phys. **77**, 935 (2005).
 - ³ F. Bergeret, A. Volkov, and K. Efetov, Rev. Mod. Phys. **77**, 1321 (2005).
 - ⁴ F. S. Bergeret, A. F. Volkov, and K. B. Efetov, Phys. Rev. B **64**, 134506 (2001).
 - ⁵ J. Linder, M. Zareyan, and A. Sudbo, Phys. Rev. B **79**, 064514 (2009).
 - ⁶ V. V. Ryazanov, V. A. Oboznov, A. Y. Rusanov, A. V. Veretennikov, A. A. Golubov, and J. Aarts, Phys. Rev. Lett. **86**, 2427 (2001).
 - ⁷ V. A. Oboznov, V. V. Bol'ginov, A. K. Feofanov, V. V. Ryazanov, and A. I. Buzdin, Phys. Rev. Lett. **96**, 197003 (2006).
 - ⁸ Y. Blum, A. Tsukernik, M. Karpovski, and A. Palevski, Phys. Rev. Lett. **89**, 187004 (2002).
 - ⁹ H. Sellier, C. Baraduc, F. Lefloch, and R. Calemczuk, Phys. Rev. B **68**, 054531 (2003).
 - ¹⁰ F. Born, M. Siegel, E. K. Hollmann, H. Braak, A. A. Golubov, D. Y. Gusakova, and M. Y. Kupriyanov, Phys. Rev. B **74**, 140501 (2006).
 - ¹¹ M. Weides, M. Kemmler, E. Goldobin, D. Koelle, R. Kleiner, H. Kohlstedt, and A. Buzdin, Appl. Phys. Lett. **89**, 122511 (2006).
 - ¹² M. Weides, M. Kemmler, H. Kohlstedt, R. Waser, D. Koelle, R. Kleiner, and E. Goldobin, Phys. Rev. Lett. **97**, 247001 (2006).
 - ¹³ J. Pfeiffer, M. Kemmler, D. Koelle, R. Kleiner, E. Goldobin, M. Weides, A. K. Feofanov, J. Lisenfeld, and A. V. Ustinov, Phys. Rev. B **77**, 214506 (2008).
 - ¹⁴ J. W. A. Robinson, S. Piano, G. Burnell, C. Bell, and M. G. Blamire, Phys. Rev. Lett. **97**, 177003 (2006).
 - ¹⁵ J. W. A. Robinson, S. Piano, G. Burnell, C. Bell, and M. G. Blamire, Phys. Rev. B **76**, 094522 (2007).
 - ¹⁶ K. D. Usadel, Phys. Rev. Lett. **25**, 507 (1970).
 - ¹⁷ G. Eilenberger, Z. Phys. **214**, 195 (1968).
 - ¹⁸ A. I. Buzdin, L. Bulaevskii, and S. Panyukov, JETP Lett. **35**, 178 (1982), Pis'ma v ZhETF **35**, 147 (1982).
 - ¹⁹ A. Buzdin, B. Bujicic, and M. Kupriyanov, JETP **74**, 124 (1992), Zh. Eksp. Teor. Fiz. **101**, 231 (1992).
 - ²⁰ E. Terzioglu and M. R. Beasley, IEEE Trans. Appl. Supercond. **8**, 48 (1998).
 - ²¹ L. B. Ioffe, V. B. Geshkenbein, M. V. Feigel'man, A. L. Fauchère, and G. Blatter, Nature (London) **398**, 679 (1999).
 - ²² A. V. Ustinov and V. K. Kaplunenko, J. Appl. Phys. **94**, 5405 (2003).
 - ²³ G. P. Pepe, R. Latempa, L. Parlato, A. Ruotolo, G. Ausanio, G. Peluso, A. Barone, A. A. Golubov, Y. V. Fominov, and M. Y. Kupriyanov, Phys. Rev. B **73**, 054506 (2006).
 - ²⁴ A. V. Zaitsev, JETP **59**, 1015 (1984), Zh. Exp. Teor. Fiz. **86**, 1742 (1984).
 - ²⁵ Z. Radovic, N. Lazarides, and N. Flytzanis, Phys. Rev. B **68**, 014501 (2003).
 - ²⁶ L. F. Mattheiss, Phys. Rev. B **1**, 373 (1970).
 - ²⁷ V. Shelukhin, A. Tsukernik, M. Karpovski, Y. Blum, K. B. Efetov, A. F. Volkov, T. Champel, M. Eschrig, T. Löfwander, G. Schön, et al., Phys. Rev. B **73**, 174506 (2006).
 - ²⁸ M. Y. Kupriyanov and V. F. Lukichev, Sov. Phys. JETP **67**, 1163 (1988).
 - ²⁹ L. Landau and E. Lifshits, Quantum Mechanics (Pergamon Press, Oxford, 1961).
 - ³⁰ A. I. Larkin and Y. N. Ovchinnikov, JETP **47**, 762 (1965), [Zh. Eksp. Teor. Fiz. **20** 1136 (1964)].
 - ³¹ P. Fulde and R. A. Ferrell, Phys. Rev. **135**, A550 (1964).
 - ³² A. Vedyayev, C. Lacroix, N. Pugach, and N. Ryzhanova,

- Europhys. Lett. **71**, 679 (2005).
- ³³ Z. Radović, L. Dobrosavljević-Grujić, and B. Vujičić, Phys. Rev. B **63**, 214512 (2001).
- ³⁴ F. Korschelle, J. Cayssol, and A. I. Buzdin, Phys. Rev. B **78**, 134505 (2008).
- ³⁵ M. Zareyan, W. Belzig, and Y. V. Nazarov, Phys. Rev. Lett. **86**, 308 (2001).
- ³⁶ D. Yu. Guskova, A. A. Golubov, and M. Y. Kupriyanov, JETP Lett. **83**, 418 (2006), [Pis'ma v ZhETF **83**, 487 (2006)].
- ³⁷ A. F. Volkov, F. S. Bergeret, and K. B. Efetov (2006), arXiv:cond-mat/0606528v1 [cond-mat.supr-con].
- ³⁸ A. S. Vasenko, A. A. Golubov, M. Y. Kupriyanov, and M. Weides, Phys. Rev. B **77**, 134507 (2008).
- ³⁹ A. A. Bannykh, J. Pfeiffer, V. S. Stolyarov, I. E. Batov, V. V. Ryazanov, and M. Weides, Phys. Rev. B **79**, 054501 (2009).
- ⁴⁰ M. Weides, Appl. Phys. Lett. **93**, 052502 (2008).
- ⁴¹ L. Neel, Compt. Rend. **237**, 1613 (1953).
- ⁴² L. Maissel and R. Glang, eds., Handbook of thin film technology (McGraw Hill Hook company, 1970).
- ⁴³ N. G. Pugach, M. Y. Kupriyanov, A. V. Vedyayev, C. Lacroix, E. Goldobin, D. Koelle, R. Kleiner, and A. S. Sidorenko, Phys. Rev. B **80**, 134516 (2009).
- ⁴⁴ A. Buzdin, JETP Lett. **78**, 1073 (2003).